Letter

Tracking the surface atomic motion in a coherent phonon oscillation

Davide Curcio,[1,*] Klara Volckaert,[1,*] Dmytro Kutnyakhov,[2] Steinn Ymir Agustsson,[3] Kevin Bühlmann,[4] Federico Pressacco,[2] Michael Heber,[2] Siarhei Dziarzhytski,[2] Yves Acremann,[4] Jure Demsar,[3] Wilfried Wurth,[2,5,†] Charlotte E. Sanders,[6] and Philip Hofmann[1,‡]

[1]*Department of Physics and Astronomy, Interdisciplinary Nanoscience Center (iNANO), Aarhus University, 8000 Aarhus C, Denmark*
[2]*Deutsches Elektronen-Synchrotron DESY, Notkestr. 85, 22607 Hamburg, Germany*
[3]*Johannes Gutenberg-Universität, Institut für Physik, 55099 Mainz, Germany*
[4]*Department of Physics, Laboratory for Solid State Physics, ETH Zürich, Otto-Stern-Weg 1, 8093 Zürich, Switzerland*
[5]*Center for Free-Electron Laser Science CFEL, Hamburg University, Luruper Chausee 149, 22761 Hamburg, Germany*
[6]*STFC Central Laser Facility, Research Complex at Harwell, Harwell Campus, Didcot OX11 0QX, United Kingdom*

(Received 25 May 2022; revised 20 October 2022; accepted 16 November 2022; published 30 November 2022)

X-ray photoelectron diffraction is a powerful tool for determining the structure of clean and adsorbate-covered surfaces. Extending the technique into the ultrafast time domain will open the door to studies as diverse as the direct determination of the electron-phonon coupling strength in solids and the mapping of atomic motion in surface chemical reactions. Here we demonstrate time-resolved photoelectron diffraction using ultrashort soft x-ray pulses from the free electron laser FLASH. We collect Se 3*d* photoelectron diffraction patterns over a wide angular range from optically excited Bi_2Se_3 with a time resolution of 140 fs. Combining these with multiple scattering simulations allows us to track the motion of near-surface atoms within the first 3 ps after triggering a coherent vibration of the A_{1g} optical phonons. Using a fluence of 4.2 mJ/cm^2 from a 1.55 eV pump laser, we find the resulting coherent vibrational amplitude in the first two interlayer spacings to be on the order of 0.01 Å.

DOI: 10.1103/PhysRevB.106.L201409

The study of ultrafast dynamics in solids has not only provided an unprecedented insight into interactions between different degrees of freedom [1–3], it has also introduced methods for preparing entirely new transient quantum states [4]. Typical experiments use optical and UV lasers for pump-probe experiments, revealing the time-resolved electronic and optical properties for a wide range of solids, from bulk materials to two-dimensional layers [5,6]. Ultrafast structural determination, on the other hand, is far less developed. Time-resolved (TR) variants of traditional x-ray diffraction (XRD) harbor a huge potential [3,7] but their use is restricted by several factors. One is the scarcity of ultrafast x-ray sources, something that is beginning to change. Another is the bulk sensitivity of XRD that is ill-matched with the more surface-localized optical pump excitation or, indeed, the extreme surface sensitivity of time- and angle-resolved photoelectron spectroscopy (TR-ARPES) used to study the electron dynamics that accompanies any structural changes. For instance, the phonon-driven modulations in the electronic structure measured by TR-ARPES can give a direct and detailed insight into the electron-phonon coupling of the system [8,9] but only under the condition that the phonon-induced structural changes *at the surface* are precisely known.

A promising complementary technique to TR-XRD is TR-x-ray photoelectron diffraction (TR-XPD). Static XPD is based on x-ray photoelectron spectroscopy (XPS) and inherits the chemical resolution and surface sensitivity from this technique: It should thus be possible to measure atomic displacements at the very surface of a solid, where they are most relevant for a comparison to TR-ARPES data. The principle of TR-XPD is illustrated in Fig. 1(a). A solid is excited by an optical pump pulse, followed by an x-ray pulse leading to the emission of a core electron. This electron can reach the detector directly or along different scattering pathways, and the measured intensity results from the coherent superposition of the direct and scattered wave field amplitudes. The diffraction pattern measured at the detector is a fingerprint of the local atomic arrangement around the emitting atom and the structure can be determined by a comparison to multiple-scattering calculations [10–13]. Unlike XRD, XPD does not rely on long-range order and it has been used to study both long-range and local phenomena such as surface relaxations [14] and geometric changes during surface reactions [15]. TR-XPD using a pulsed x-ray source thus holds promise for real-time investigations for a wide range of phenomena. In fact, first TR-XPD demonstrations have been given for simple systems such as aligned molecules [16,17]. The effect has also been observed for solid surfaces [18,19], but a rigorous structural determination based on such data is still missing.

Here we demonstrate the power of TR-XPD to track the ultrafast dynamic changes in the surface structure upon the excitation of coherent phonons on the (111) surface of the topological insulator Bi_2Se_3. Symmetric A_{1g} coherent optical phonons can be launched [20,21] and controlled [22] by ul-

*These two authors contributed equally to this work.
†Deceased.
‡philip@phys.au.dk

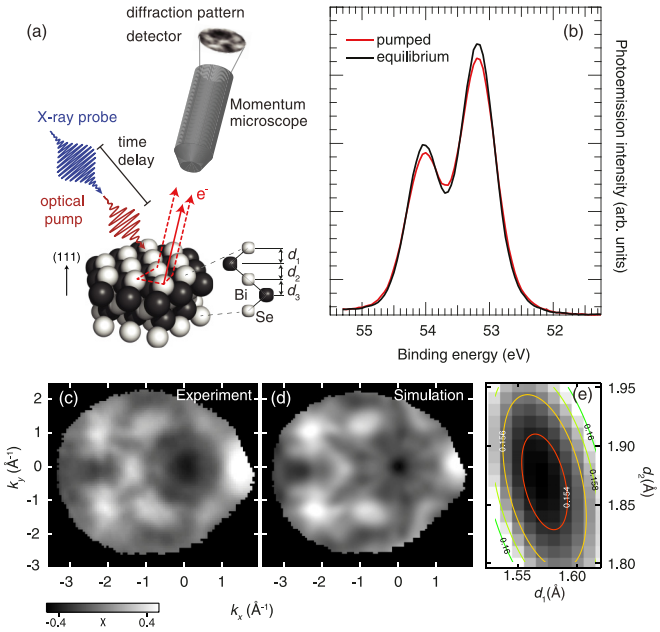

FIG. 1. (a) Principle of TR-XPD. A solid is excited with a short low-energy light pulse, followed by a soft x-ray pulse that gives rise to photoemission from core levels. The core level photoemission intensity shows an angular distribution that is given by the coherent interference of the photoelectrons' partial waves reaching the detector along different pathways, either directly (solid line) or via multiple-scattering events (dashed lines). The crystallographic direction of the surface normal is indicated on the left-hand side. (b) Se $3d$ core level spectrum before and after optical excitation. (c) Se $3d$ modulation function, obtained for integrated times of $t < -0.075$ ps. The scale bar applies to both panels (c) and (d). (d) Calculated modulation function for the best-fit structure. (e) Reliability factor for the comparison between experimental and theoretical modulation functions as a function of the first two interlayer distances d_1 and d_2. The contours represent a fit to a two-dimensional polynomial.

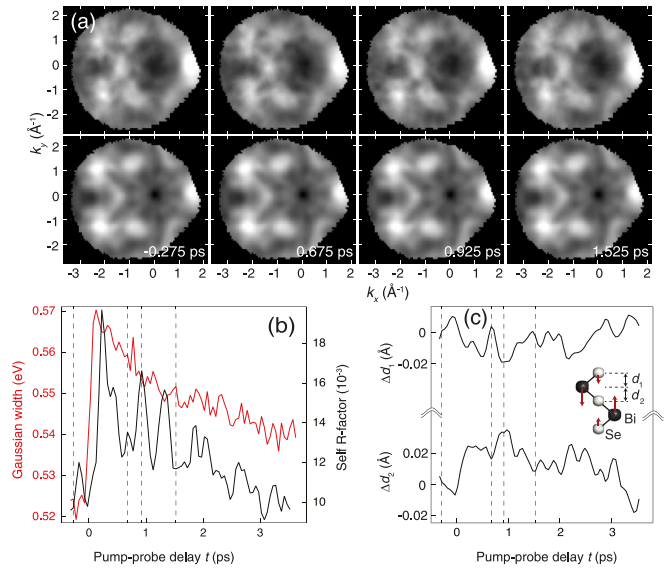

FIG. 2. Time-dependent structural analysis. (a) Top row: TR-XPD patterns integrated over an interval of 60 fs around selected time delays. Bottom row: Best-fit calculated patterns, fitting only the parameters $\Delta d_1(t)$ and $\Delta d_2(t)$, i.e., the deviation of the interlayer spacings from the equilibrium position. (b) Black: self-R factor of TR-XPD patterns with equilibrium pattern in Fig 1(c). Red: Gaussian width of Se $3d_{5/2}$ line. (c) Time-dependent interlayer distance changes $\Delta d_1(t)$ and $\Delta d_2(t)$. The inset shows the displacement for an A_{1g}^1 phonon (red arrows). The dashed lines in (b) and (c) indicate the time delays for the images in (a).

trashort optical laser pulses. The A_{1g}^1 phonon relevant to the present study has a frequency on the order of 2 THz and decays with a time constant of ≈3 ps [22]. The excitation of coherent phonons leads to small time-dependent variations in the binding energy of the electronic surface and bulk states, as measured by TR-ARPES [23]. The bulk states show a binding energy oscillation consistent with the A_{1g}^1 mode, whereas the surface state energy modulation can only be described by superimposing a second vibration of a slightly lower frequency (2.05 THz instead of 2.23 THz) [23]. This is consistent with a softening of force constants near the surface and the presence of a surface-localized vibrational mode [24].

TR-XPD experiments on the Se $3d$ core levels of Bi_2Se_3 have been performed with the HEXTOF experimental station at the PG2 beamline of the free electron laser FLASH [25,26]. Samples were cleaved in vacuum and held at room temperature during the measurements. The pump photon energy and fluence were 1.55 eV and ≈4.2 mJ cm^{-2}, respectively. The probe photon energy was 113 eV. Major challenges for TR-XPD are the need to collect high-quality TR-XPS spectra, not only integrated over the detector but for all emission angles individually. This necessitated a total data collection time of ≈19 h. After correcting for jitter from FLASH, the time resolution was 140 fs. For these and other experimental details, see the Supplemental Material (SM) [27] and Refs. [28–34].

Figure 1(b) shows the effect of optical pumping on the Se $3d$ core level line shape. There is a small but clear difference between the spectrum collected before the arrival of the pump pulse (black) and the spectrum at peak excitation (red). The spectra could be fitted by a Doniach-Šunjić line shape [35] with a very small asymmetry (see SM [27]). Pumping the material leads to a small increase in the Gaussian linewidth that could be used to estimate the experimental time resolution [see Fig. 2(b)]. However, the effect is much smaller than in other materials [36,37].

TR-XPD patterns were obtained from the fits as the area under the Se $3d$ peak, using Gaussian binning of the photoemission intensity as described in the SM [27]. Instead of representing the XPD pattern as the $\mathbf{k}$-dependent Se $3d$ photoemission intensity $I(\mathbf{k})$, we use the so-called modulation function defined by $\chi(\mathbf{k}) = [I(\mathbf{k}) - I_0(\mathbf{k})]/I_0(\mathbf{k})$, where $I_0(\mathbf{k})$ is a two-dimensional polynomial [10,27]. This modulation function is displayed in Fig. 1(c) for the photoemission intensity in the unexcited state: It is obtained by integrating the data at time delays $t < -0.075$ ps, where $t = 0$ corresponds to the highest temporal overlap of the pump and probe pulses; and negative values correspond to the probe pulse arriving before the pump pulse.

Before addressing the time-resolved atomic motion after an optical excitation, we determine the quasistatic geometric structure of Bi_2Se_3 by comparing the equilibrium XPD pattern

in Fig. 1(c) to multiple scattering calculations performed by the software package for electron diffraction in atomic clusters [38]. The calculated modulation function for the optimized structural and nonstructural parameters is given in Fig. 1(d) [27]. The agreement with the experimental result is excellent. To quantify this, the two modulation functions can be compared by the reliability factor

$$R = \frac{\sum_i (\chi_{e,i} - \chi_{t,i})^2}{\sum_i \left(\chi_{e,i}^2 + \chi_{t,i}^2\right)}, \tag{1}$$

where $\chi_{e,i}$ and $\chi_{t,i}$ are the experimental and theoretical modulation functions for the ith $\mathbf{k}$ point, respectively. We find a very low value of $R = 0.15$. In order to reach this agreement, the structural parameters were initially fixed to the bulk values for Bi_2Se_3 [39]. An optimization was limited to the first three interlayer distances d_1, d_2, and d_3, as defined in Fig. 1(a). Changing deeper interlayer distances had a negligible effect on the resulting R factor. R is plotted as a function of d_1 and d_2 in Fig. 1(e). The values of R are fitted to a three-dimensional paraboloid in order to determine the optimum parameters d_1 to d_3 with a higher precision than given by the grid of R calculations. The best agreement between experiment and calculation is found for $d_1 = 1.579 \pm 0.050$ Å, $d_2 = 1.866 \pm 0.100$ Å, and $d_3 = 1.980 \pm 0.100$ Å. The uncertainties are determined from the variance of the R factor [27,40]. With respect to the bulk structural parameters, there is a small inward relaxation of the first interlayer spacing, in excellent agreement with a previous surface structure determination by surface XRD and low-energy electron diffraction [41], and in fair agreement with a static XPD investigation [14]. The second interlayer spacing also shows a small inward relaxation, whereas in previous experiments [14,41] it was found to be very similar to the bulk value. The third interlayer spacing is found to show negligible relaxation. For more details on the multiple scattering simulations, see the SM [27].

The average structure is now taken as a starting point to determine the time-dependent changes of d_1 to d_3 after the optical excitation. It turns out that the time-dependent variation of d_3 is much smaller than that of the other two interlayer distances. In order to avoid overfitting and instabilities in the presence of noise, d_3 is therefore set to remain at its equilibrium value. XPD patterns at selected points in time are shown in the top row of Fig. 2(a). Figure 2(b) shows a basic characterization of the time-dependent data with the vertical dashed lines corresponding to the time points chosen for the XPD patterns in panel (a). The black line is a self-R factor between experimental data alone, comparing the measured modulation function at each time delay with the static modulation function in Fig. 1(c), i.e., the modulation from the integrated data for $t < 0.075$ ps. Note that this self-R factor is defined as in Eq. (1), merely exchanging the modulation functions which are to be compared. This allows us to judge—from experimental data alone—how much the pattern changes after the optical excitation. The self-R factor shows a rapid increase shortly after $t = 0$, followed by a gradual decay as the surface relaxes back to its equilibrium structure (there can be additional changes of the overall lattice constant due to the induced carriers over a much larger timescale than investigated here [42]). The decay is superimposed with a pronounced oscillatory structure, indicating that the path back to equilibrium is accompanied by periodic structural changes, such as optical phonons. Figure 2(b) also gives the time-dependent Gaussian width of the Se $3d_{5/2}$ peak. This shows stepwise broadening at $t = 0$, followed by a gradual narrowing. The width of the step establishes the time resolution of the experiment. It is clearly significantly shorter than the period of the observed oscillations.

A quantitative structural analysis is now performed by comparing the time-resolved diffraction patterns to multiple scattering simulations like the one in Fig. 1(d), while optimizing the structural parameters (d_1 and d_2) for each time delay, using a two-dimensional interpolation of R as in Fig. 1(e). The resulting changes for the two interlayer distances with respect to the equilibrium values (Δd_1 and Δd_2) are shown in Fig. 2(c) and the best fits to the measured XPD patterns are given in the lower row of Fig. 2(a). Both Δd_1 and Δd_2 show clear oscillations with an amplitude on the order of 0.01 Å, especially immediately after excitation and towards the end of the explored time interval. The period of the oscillation is about 500 fs, consistent with the expected excitation of an A_{1g}^1 optical phonon. The structural changes are also in line with what is expected for an A_{1g}^1 phonon. As seen in the inset, this phonon mode involves the simultaneous movement of the two outer layers (Bi and Se) in a quintuple layer (QL) with respect to the static central Se layer. The changes in d_1 and d_2 should thus be correlated and be either in phase or out of phase, depending on the relative size of the movements in the first and second layer atoms. The in-phase (out-of-phase) motion corresponds to a larger (smaller) displacement of the outer Se atom from the central atom than the displacement of the Bi atom. Figure 2(c) shows the displacements to be approximately out of phase.

The structural changes should be treated with some caution. As seen in Fig. 2(a), the changes in the diffraction pattern are very small. The changes in d_1 and d_2 have the expected order of magnitude [8,43] but they are much smaller than the uncertainties for the determination of the static values of the interlayer distances. We can thus expect that some of the movements seen in Fig. 2(c) are due to noise. On the other hand, we need to keep in mind that uncertainties stated for the static structural parameters also account for systematic errors, for example from oversimplifications in the multiple scattering simulations. Such effects limit the overall reachable agreement (and hence, the uncertainties) but they are identical for the calculations performed at each point in time, suggesting that the changes in d_1 and d_2 should be more reliable than their absolute values. The purely statistical uncertainties due to noisy data can be estimated from the structural fluctuations for negative time delays in Fig. 2(c) and these are much smaller than the static uncertainties and also smaller than the pronounced structural oscillations at later time delays. Finally, a structural change is supported by the oscillatory shape of the time-dependent R factor in Fig. 2(b) and the fact that both the oscillation frequency and the movements in d_1 and d_2 are consistent with an excited A_{1g}^1 optical phonon.

For a more detailed understanding of the observed structural changes, we introduce a minimal one-dimensional model to study time-dependent interlayer distances near the surface.

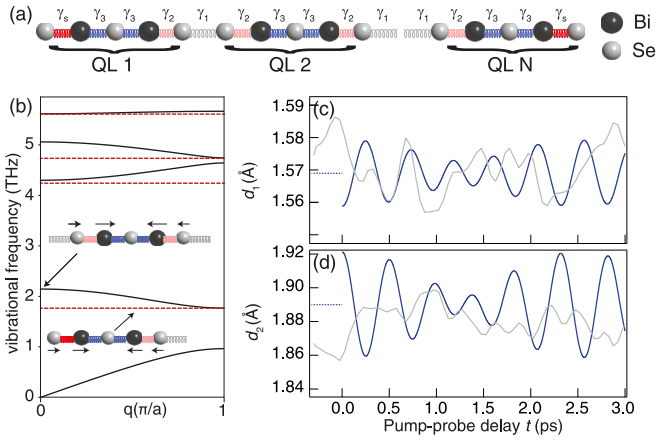

FIG. 3. (a) One-dimensional linear chain model with five atoms per unit cell and nearest neighbor interactions. The bulk is described by three force constants $\gamma_{1,2,3}$. The first layer force constant is permitted to be different (γ_{1s}). (b) Phonon dispersion curves for the bulk (black solid lines) and the surface-localized modes (red dashed lines). (c) and (d) Dark-blue line: Time-dependent displacement of the first and second atomic spacing in the one-dimensional chain, respectively, when exciting both the bulk A_{1g}^1 mode and the A_{1g}^1 derived end mode for d_1 (c) and d_2 (d). The dashed lines before $t = 0$ represent the equilibrium values of the linear chain model. Light-gray line: experimental displacements from Fig. 2(c).

The model is illustrated in Fig. 3(a). We consider a linear chain of atoms with a Se-Bi-Se-Bi-Se QL as the basis. The model has three different spring constants, γ_2 and γ_3 within a unit cell and a weaker γ_1 between the unit cells, representing the van der Waals forces between the QLs of Bi_2Se_3. We adjust the force constants such that the phonon dispersion is similar to that of Bi_2Se_3 in the Γ-Z direction of the bulk Brillouin zone [see Fig. 3(b)] [24,44]. The A_{1g}^1 phonon mode corresponds to the lowest optical branch at the zone center. Its displacement pattern is shown in the inset. In the model, the vibrational amplitude for the second layer Bi atoms is higher than that of the first layer Se atoms, consistent with an out-of-phase motion of d_1 and d_2. Using the bulk force constants does not give rise to distinct vibrations at the end of the chain. We therefore introduce a localized end mode by choosing a softer force constant γ_s at the end of the chain (reduced by 10% with respect to γ_2). This results in several end-localized modes with frequencies that do not appear in the bulk continuum [dashed red lines in Fig. 3(b)]. The displacement pattern of the A_{1g}^1-derived end mode is also given as an inset. Its slight asymmetry is caused by the the softer γ_s and the missing spring at the end of the chain.

Using a superposition of the A_{1g}^1 bulk and end modes, it is possible to achieve a qualitative agreement with the experimentally observed displacements, as shown in Figs. 3(c) and 3(d). In this picture, the reduced vibrational amplitude in the middle of the investigated delay time window is the result of a beating pattern of the two modes. The very simple model can of course not be expected to give a quantitative description of $d_1(t)$ and $d_2(t)$ and there is some freedom to choose the best parameters for reproducing the experimental displacements (the relative excitation strength and the phase between the modes; see SM [27]).

In summary, we have demonstrated the use of TR-XPD for an ultrafast tracking of the surface atomic structure after the excitation of a coherent phonon in Bi_2Se_3. The coherent vibrational amplitudes for the pump fluence used here are on the order of 0.01 Å, allowing the calculation of the deformation potential when combined with TR-ARPES experiments. An important challenge for TR-XRD is the need for high-quality XPS spectra when binning the collected data in both **k** and time. This leads to very long data acquisition times and, in our case, limits the length of the delay time interval that can be studied and the precision of the obtained structural parameters. The bottleneck in the data acquisition is vacuum space charge [45] and a desirable characteristic of future free electron laser sources will be a much increased pulse repetition rate. This will allow similar studies not only to take data sets of better quality and over longer time delays but also at multiple photon energies, drastically increasing the precision of the structural determination. Eventually, the chemical and local sensitivity of TR-XPD could be exploited, e.g., to probe the detailed atomic motion in specific coherently excited vibrational modes in molecules, representing a time-resolved version of the previously suggested use of XPD to measure the time-averaged probability distribution of atoms [46].

This work was supported by VILLUM FONDEN via the Centre of Excellence for Dirac Materials (Grant No. 11744) and the Independent Research Fund Denmark (Grant No. 1026-00089B). This research was carried out at FLASH at DESY, a member of the Helmholtz Association. The research leading to these results has been supported by the project CALIPSOplus under Grant Agreement No. 730872 from the EU Framework Programme for Research and Innovation HORIZON 2020, by the Deutsche Forschungsgemeinschaft (DFG) within the framework of the Collaborative Research Centre SFB 925-170620586 (project B2), and within TRR 173-268565370 (Project No. A05). We thank Holger Meyer, Sven Gieschen, and Harald Redlin for experimental support, as well as Gerd Schönhense, Davide Campi, Anton Tamögl, and Wolfgang Ernst for helpful discussions.

[1] A. Kirilyuk, A. V. Kimel, and T. Rasing, Rev. Mod. Phys. **82**, 2731 (2010).
[2] C. Giannetti, M. Capone, D. Fausti, M. Fabrizio, F. Parmigiani, and D. Mihailovic, Adv. Phys. **65**, 58 (2016).
[3] M. Buzzi, M. Först, R. Mankowsky, and A. Cavalleri, Nat. Rev. Mater. **3**, 299 (2018).
[4] A. de la Torre, D. M. Kennes, M. Claassen, S. Gerber, J. W. McIver, and M. A. Sentef, Rev. Mod. Phys. **93**, 041002 (2021).
[5] M. Maiuri, M. Garavelli, and G. Cerullo, J. Am. Chem. Soc. **142**, 3 (2020).
[6] U. Bovensiepen and P. S. Kirchmann, Laser Photonics Rev. **6**, 589 (2012).

[7] A. M. Lindenberg, S. L. Johnson, and D. A. Reis, Annu. Rev. Mater. Res. **47**, 425 (2017).

[8] S. Gerber, S.-L. Yang, D. Zhu, H. Soifer, J. A. Sobota, S. Rebec, J. J. Lee, T. Jia, B. Moritz, C. Jia *et al.*, Science **357**, 71 (2017).

[9] U. De Giovannini, H. Hübener, S. A. Sato, and A. Rubio, Phys. Rev. Lett. **125**, 136401 (2020).

[10] D. P. Woodruff, in *Angle-Resolved Photoemission*, edited by S. D. Kevan, Studies in Surface Science and Catalysis Vol. 74 (Elsevier, Amsterdam, 1992), pp. 243–290.

[11] D. P. Woodruff and A. M. Bradshaw, Rep. Prog. Phys. **57**, 1029 (1994).

[12] J. Osterwalder, P. Aebi, R. Fasel, D. Naumovic, P. Schwaller, T. Kreutz, L. Schlapbach, T. Abukawa, and S. Kono, Surf. Sci. **331-333**, 1002 (1995).

[13] P. Hofmann, K.-M. Schindler, S. Bao, A. M. Bradshaw, and D. P. Woodruff, Nature (London) **368**, 131 (1994).

[14] M. V. Kuznetsov, L. V. Yashina, J. Sánchez-Barriga, I. I. Ogorodnikov, A. S. Vorokh, A. A. Volykhov, R. J. Koch, V. S. Neudachina, M. E. Tamm, A. P. Sirotina *et al.*, Phys. Rev. B **91**, 085402 (2015).

[15] S. Bao, P. Hofmann, K. M. Schindler, V. Fritzsche, A. M. Bradshaw, D. P. Woodruff, C. Casado, and M. C. Asensio, J. Phys.: Condens. Matter **6**, L93 (1994).

[16] R. Boll, A. Rouzée, M. Adolph, D. Anielski, A. Aquila, S. Bari, C. Bomme, C. Bostedt, J. D. Bozek, H. N. Chapman *et al.*, Faraday Discuss. **171**, 57 (2014).

[17] G. Kastirke, M. S. Schöffler, M. Weller, J. Rist, R. Boll, N. Anders, T. M. Baumann, S. Eckart, B. Erk, A. De Fanis *et al.*, Phys. Rev. X **10**, 021052 (2020).

[18] M. Greif, L. Kasmi, L. Castiglioni, M. Lucchini, L. Gallmann, U. Keller, J. Osterwalder, and M. Hengsberger, Phys. Rev. B **94**, 054309 (2016).

[19] A. K. R. Ang, Y. Fukatsu, K. Kimura, Y. Yamamoto, T. Yonezawa, H. Nitta, A. Fleurence, S. Yamamoto, I. Matsuda, Y. Yamada-Takamura *et al.*, Jpn. J. Appl. Phys. **59**, 100902 (2020).

[20] J. Qi, X. Chen, W. Yu, P. Cadden-Zimansky, D. Smirnov, N. H. Tolk, I. Miotkowski, H. Cao, Y. P. Chen, Y. Wu *et al.*, Appl. Phys. Lett. **97**, 182102 (2010).

[21] N. Kumar, B. A. Ruzicka, N. P. Butch, P. Syers, K. Kirshenbaum, J. Paglione, and H. Zhao, Phys. Rev. B **83**, 235306 (2011).

[22] J. Hu, K. Igarashi, T. Sasagawa, K. G. Nakamura, and O. V. Misochko, Appl. Phys. Lett. **112**, 031901 (2018).

[23] J. A. Sobota, S.-L. Yang, D. Leuenberger, A. F. Kemper, J. G. Analytis, I. R. Fisher, P. S. Kirchmann, T. P. Devereaux, and Z.-X. Shen, Phys. Rev. Lett. **113**, 157401 (2014).

[24] A. Ruckhofer, D. Campi, M. Bremholm, P. Hofmann, G. Benedek, M. Bernasconi, W. E. Ernst, and A. Tamtögl, Phys. Rev. Res. **2**, 023186 (2020).

[25] D. Kutnyakhov, R. P. Xian, M. Dendzik, M. Heber, F. Pressacco, S. Y. Agustsson, L. Wenthaus, H. Meyer, S. Gieschen, G. Mercurio *et al.*, Rev. Sci. Instrum. **91**, 013109 (2020).

[26] N. Gerasimova, S. Dziarzhytski, and J. Feldhaus, J. Mod. Opt. **58**, 1480 (2011).

[27] See Supplemental Material at http://link.aps.org/supplemental/10.1103/PhysRevB.106.L201409 for details on the pump and probe laser characteristics, jitter correction, energy and momentum axis calibration, distortion corrections, data binning and data quality, XPS data fitting and XPD patterns, multiple-scattering simulations, and the one-dimensional phonon model.

[28] M. Martins, M. Wellhöfer, J. T. Hoeft, W. Wurth, J. Feldhaus, and R. Follath, Rev. Sci. Instrum. **77**, 115108 (2006).

[29] G. Schönhense, K. Medjanik, C. Tusche, M. de Loos, B. van der Geer, M. Scholz, F. Hieke, N. Gerken, J. Kirschner, and W. Wurth, Ultramicroscopy **159**, 488 (2015).

[30] G. Schönhense, D. Kutnyakhov, F. Pressacco, M. Heber, N. Wind, S. Y. Agustsson, S. Babenkov, D. Vasilyev, O. Fedchenko, S. Chernov *et al.*, Rev. Sci. Instrum. **92**, 053703 (2021).

[31] H. Redlin, A. Al-Shemmary, A. Azima, N. Stojanovic, F. Tavella, I. Will, and S. Düsterer, Nucl. Instrum. Methods Phys. Res., Sect. A **635**, S88 (2011).

[32] S. V. Hoffmann, C. Søndergaard, C. Schultz, Z. Li, and P. Hofmann, Nucl. Instrum. Methods Phys. Res., Sect. A **523**, 441 (2004).

[33] O. Madelung, *Semiconductors: Data Handbook* (Springer Science & Business Media, Berlin, 2004).

[34] S. Tanuma, C. J. Powell, and D. R. Penn, Surf. Interface Anal. **21**, 165 (1994).

[35] S. Doniach and M. Sunjic, J. Phys. C **3**, 285 (1970).

[36] M. Dendzik, R. P. Xian, E. Perfetto, D. Sangalli, D. Kutnyakhov, S. Dong, S. Beaulieu, T. Pincelli, F. Pressacco, D. Curcio *et al.*, Phys. Rev. Lett. **125**, 096401 (2020).

[37] D. Curcio, S. Pakdel, K. Volckaert, J. A. Miwa, S. Ulstrup, N. Lanatà, M. Bianchi, D. Kutnyakhov, F. Pressacco, G. Brenner *et al.*, Phys. Rev. B **104**, L161104 (2021).

[38] F. J. García de Abajo, M. A. Van Hove, and C. S. Fadley, Phys. Rev. B **63**, 075404 (2001).

[39] S. Nakajima, J. Phys. Chem. Solids **24**, 479 (1963).

[40] H. Bana, E. Travaglia, L. Bignardi, P. Lacovig, C. E. Sanders, M. Dendzik, M. Michiardi, M. Bianchi, D. Lizzit, F. Presel *et al.*, 2D Mater. **5**, 035012 (2018).

[41] D. D. dos Reis, L. Barreto, M. Bianchi, Guilherme Almeida Silva Ribeiro, E. A. Soares, W. S. Silva, V. E. de Carvalho, J. Rawle, M. Hoesch, C. Nicklin *et al.*, Phys. Rev. B **88**, 041404(R) (2013).

[42] S. Kim, Y. Kim, J. Kim, S. Choi, K. Yun, D. Kim, S. Y. Lim, S. Kim, S. H. Chun, J. Park *et al.*, Nano Lett. **21**, 8554 (2021).

[43] S. L. Johnson, P. Beaud, E. Möhr-Vorobeva, A. Caviezel, G. Ingold, and C. J. Milne, Phys. Rev. B **87**, 054301 (2013).

[44] X. Zhu, L. Santos, R. Sankar, S. Chikara, C. Howard, F. C. Chou, C. Chamon, and M. El-Batanouny, Phys. Rev. Lett. **107**, 186102 (2011).

[45] B. Schönhense, K. Medjanik, O. Fedchenko, S. Chernov, M. Ellguth, D. Vasilyev, A. Oelsner, J. Viefhaus, D. Kutnyakhov, W. Wurth *et al.*, New J. Phys. **20**, 033004 (2018).

[46] P. Hofmann, O. Schaff, and K. M. Schindler, Phys. Rev. Lett. **76**, 948 (1996).